International Journal of Mathematical Archive-8(1), 2017, 109-125
Available online through www.ijma.info ISSN 2229 – 5046

FLOW AND THERMAL CONVECTION OF THIRD GRADE VISCOELASTIC FLUID FROM A VERTICAL POROUS PLATE WITH BIOT NUMBER EFFECTS

R BHUVANA VIJAYA[1], S ABDUL GAFFAR[2], K VENKATADRI[1] AND B MD HIDAYATHULLA KHAN[*1]

[1]Department of Mathematics, Jawaharlal Nehru Technological University, Anantapur-515 002, India.

[2]Department of Mathematics, Salalah College of Technology,Salalah, Oman.

(Received On: 13-12-16; Revised & Accepted On: 19-01-17)

ABSTRACT

A *mathematical model is developed to analyse the nonlinear, non-isothermal, steady-state, laminar boundary layer flow and heat transfer of an incompressible third grade viscoelastic non-Newtonian fluid past a vertical porous plate with Biot number effects. The transformed conservation equations of mass, linear momentum and heat equations are solved numerically subject to physically appropriate boundary conditions using a second-order accurate implicit finite-difference Keller-Box method (**KBM**). The influence of a number of emerging non-dimensional parameters, namely the third grade fluid parameter (ϕ), material fluid parameters (ε_1, ε_2), Prandtl number (Pr), Biot number (γ) and dimensionless tangential coordinate (ξ) on velocity and temperature evolution in the boundary layer regime are examined in detail. Furthermore, the effects of these parameters on surface heat transfer rate and local skin friction are also investigated. It is observed that velocity, skin friction and heat transfer rate are reduced with increasing third-grade fluid parameter (ϕ), whereas the temperature is increased. An increase in the material fluid parameter (ε_1) reduces the velocity, skin friction and heat transfer rate but increases temperature. And increasing material fluid parameter (ε_2) accelerates velocity, skin friction and heat transfer rate but decelerates the temperature. Detailed interpretation of the computations is included. The present simulations are of interest in chemical engineering systems and solvent and low density polymer materials processing.*

Keywords: *Non-Newtonian third grade fluid; material fluid parameters; heat transfer rate;*

NOMENCLATURE

C_f	skin friction coefficient
f	dimensionless steam function
Gr	Grashof number
g	acceleration due to gravity
k	thermal conductivity of the third grade fluid
Nu	local Nusselt number
Pr	Prandtl number
T	temperature of the fluid
u, v	dimensionless velocity components along the x- and y- directions, respectively
V	velocity vector
x	stream wise coordinate
y	transverse coordinate

Corresponding Author: B MD Hidayathulla Khan[*1], [1]Department of Mathematics, Jawaharlal Nehru Technological University, Anantapur-515 002, India.

GREEK

α thermal diffusivity
β coefficient of thermal expansion
ε_1 first viscoelastic material fluid parameter
ε_2 second viscoelastic material fluid parameter
β_3 third grade material parameter
ν kinematic viscosity
ρ fluid density
μ Newtonian dynamic viscosity
η dimensionless radial coordinate
θ dimensionless temperature
ϕ third grade dimensionless viscoelastic fluid parameter
ξ dimensionless tangential coordinate
ψ dimensionless stream function
γ Biot number

SUBSCRIPTS

w Surface conditions on plate (wall)
∞ Free stream conditions

1. INTRODUCTION

The interest in non-Newtonian fluid dynamics continues to grow in response to increasing applications in many branches of advanced industrial technologies including thermal oil recovery, coal-oil slurries, detergent and paint production, smart coating and suspension fabrication, pharmacology, physiological transport processes (blood, bile and synovial fluid), slurry conveyance, polymer synthesis and food processing. In these applications, the working fluids are generically rheological in nature and the constitutive relationship between stress and rate of strain is non-linear in comparison to the Navier-Stokes equations (valid only for Newtonian fluids). The rheology of these fluids manifests in many complex characteristics including fading memory, relaxation, elongation stresses, spin of suspended particles, retardation and adhesion. In general, the mathematical problems in non-Newtonian fluids are more complicated as a result of strong non-linearity and higher-order of the differential transport equations compared with viscous Newtonian fluids. Despite their complexities, scientists and engineers are engaged in non-Newtonian fluid dynamics since the analysis and implementation of these fluids is critical to many diverse systems in biotechnology, chemical gels, manufacture of plastics, medical engineering etc. Although the systems of equations emerging in non-Newtonian models usually require recourse to numerical methods for a robust solution, closed-form analytical solutions have been attained in some limited cases. Both exact and numerical solutions offer a vital compliment to experimental studies and vice versa. Mathematical rheology is therefore an essential component of interpreting correctly experimental (laboratory-based) tests using for example rheometers, cone-plate devices, rod-stirring etc. Many investigations of rheological hydrodynamics have been communicated. An exact solution to the viscoelastic fluid flow induced by a circular cylinder subjected to time-dependent shear stress was derived by Fetecau *et al*. [1]. Robust solutions for unsteady helical flows of Oldroyd-B and second grade fluids were computed by Jamil *et al*. [2]. Tan and Masuoka [3, 4] discussed the stability of the Maxwell fluid in a porous medium and derived an exact solution to the Stokes first problem for an Oldroyd-B fluid. Computational methods have however dramatically extended the range of problems studied in rheological fluid mechanics and indeed have allowed the simultaneous consideration of heat and mass transfer. Such studies have successfully examined an ever-widening spectrum of non-Newtonian material models with various algorithms and have been applied in medical, energy, propulsion and other areas of engineering sciences. Representative studies in recent years include Prasad *et al.* [5] who employed the Casson yield stress model to simulate enrobing thermo-fluid dynamics of food-stuffs. Chaube *et al.* [6] applied the differential transform method and Ostwald-DeWaele power-law model to study peristaltic propulsion in variable-diameter tubes with wall hydrodynamic slip. Further studies have addressed heat and mass transfer in external boundary layer convection flow and utilized Jeffery's viscoelastic model [7] and the Eyring−Powell model [8]. All these investigations have demonstrated beyond doubt that rheology has a significant effect on thermo-fluid dynamic characteristics. These studies have also shown that the different rheological models capture different behavioural characteristics of various real liquids and that there is no single non-Newtonian model that exhibits all the properties of non-Newtonian fluids.

Most non-Newtonian models involve some form of modification to the momentum conservation equations (Newton's second law). Several fluid models have however emerged as strong candidates in successfully mimicking actual non-Newtonian characteristics. Among these, the *differential type fluid models* have proved popular. The simplest subclass of these viscoelastic models is designated the *second grade* fluid, which describes the normal stress differences but cannot predict shear thinning/thickening phenomena. However, the third-grade fluid model is capable of predicting both normal stress and shear thinning/thickening phenomena. Many researchers have examined the flows of third-grade fluids for various scenarios, usually with a mathematical emphasis and very little if any physical understanding or

interpretation of the solutions. These studies are therefore of very limited value to engineers who are the primary professionals working in complex (polymeric) fluid mechanics industries. For instance, Sahoo [9] investigated the flow and heat transfer of third grade fluid from an exponentially stretching sheet with partial slip boundary conditions. Aziz and Aziz [10] studied the magnetohydrodynamic flow of a third grade fluid in porous media with wall mass flux effects. Hayat *et al*. [11] analyzed axisymmetric flow of a magnetized third grade fluid between stretching sheets with heat transfer. Melting heat transfer in the stagnation-point flow of third grade fluid from an extending sheet with viscous dissipation was addressed by Hayat *et al.* [12] using the semi-analytical homotopy analysis method. A theoretical simulation of hydromagnetic axisymmetric flow of third grade fluid induced by a stretching cylinder was presented by Hayat *et al*. [13]. Samuel *et al.* [14] considered thermodynamic aspects of hydromagnetic third grade fluid flow in a porous media channel. Abdul hameed *et al*. [15] computed solutions for transient third-grade flow caused by the periodic motion of an infinite wall with transpiration. Rashidi *et al.* [16] conducted an entropy generation minimization analysis of convective magnetic flow of third grade non-Newtonian fluid from a stretching sheet. Again these studies *did even not attempt* to evaluate the physics of third grade fluid effects making them of minimal interest from an engineering perspective.

Convective heat transfer has also mobilized substantial interest owing to its importance in industrial and environmental technologies including energy storage, gas turbines, nuclear plants, rocket propulsion, geothermal reservoirs, photovoltaic panels etc. The convective boundary condition has also attracted some interest and this usually is simulated via a Biot number in the wall thermal boundary condition. Ishak [17] discussed the similarity solutions for flow and heat transfer over a permeable surface with convective boundary condition. Aziz [18] provided a similarity solution for laminar thermal boundary layer over a flat surface with a convective surface boundary condition. Aziz [19] further studied hydrodynamic and thermal slip flow boundary layers with an iso-flux thermal boundary condition. The buoyancy effects on thermal boundary layer over a vertical plate subject a convective surface boundary condition was studied by Makinde and Olanrewaju [20]. Further recent analyses include Makinde and Aziz [21]. Gupta *et al*. [22] used a finite element method to simulate mixed convective-radiative micropolar shrinking sheet flow with a convective boundary condition. Makinde *et al.* [23] studied cross diffusion effects and Biot number influence on hydromagnetic Newtonian boundary layer flow with homogenous chemical reactions and **MAPLE** quadrature routines. Bég *et al.* [24] analyzed Biot number and buoyancy effects on magnetohydrodynamic thermal slip flows. Subhashini *et al.* [25] studied wall transpiration and cross diffusion effects on free convection boundary layers with a convective boundary condition. S. Nadeem et al. [26] investigated the MDH three-dimensional boundary layer flow of Casson nanofluid past a linearly stretching sheet with convective boundary condition. Ammarah Raees *et al.* [27] examined the explicit solutions of wall jet flow subject to a convective boundary condition. The influence of convective boundary condition on double diffusive mixed convection from a permeable vertical surface was examined by P.M. Patil [28]. Fazlina Aman and Anuar Ishak [29] investigated the mixed convection boundary layer flow towards a vertical plate with convective surface boundary condition using the shooting technique. Mohammad M. Rashidi *et al.* [30] examined the MHD natural convection with convective surface boundary condition over a flat plate using Keller box technique. Rabia Malik *et al.* [31] studied the flow and heat transfer in Sisko fluid with convective boundary condition. O. D. Makinde and A. Aziz [32] presented the boundary layer flow of a nonfluid past a stretching sheet with a convective boundary condition using RK method.

The objective of the present study is to investigate the steady, laminar thermal convection boundary layer flow and heat transfer of a *third grade viscoelastic non-Newtonian fluid* past a vertical porous plate with Biot number effects. Appropriate non-similar transformations are deployed to render the conservation equations into dimensionless form. The emerging dimensionless partial differential equations with associated boundary conditions constitute a highly nonlinear, coupled two-point boundary value problem making exact solutions practically impossible. Keller's implicit finite difference "box" scheme is therefore implemented to obtain approximate computational solutions [33-34]. The boundary value problem features a number of dimensionless thermophysical parameters, namely *the third grade fluid parameter (ϕ), viscoelastic material fluid parameters (ε_1, ε_2), Biot number (γ) and Prandtl number (Pr).* The influence of selected parameters on velocity, temperature, skin friction and heat transfer rate (local Nusselt number) characteristics are studied. The present problem has to the authors' knowledge not appeared thus far in the scientific literature and is relevant to thermal fabrication (heat treatment) of paints sprays, waster-based rheological gel solvents and low density polymeric manufacturing processes in chemical engineering.

2. NON-NEWTONIAN CONSTITUTIVE THIRD GRADE FLUID MODEL

In the present study a subclass of non-Newtonian fluids known as the *third grade fluid* is considered. This model physically captures accurately the viscoelastic characteristics of certain polymers [35-36]. The Cauchy stress tensor of an incompressible *third grade* non-Newtonian fluid following Truesdell and Noll [37] takes the form:

$$\tau = -pI + \mu A_1 + \alpha_1 A_2 + \alpha_2 A_1^2 + \beta_1 A_3 + \beta_2 \left(A_1 A_2 + A_2 A_1 \right) + \beta_3 \left(tr A_1^2 \right) A_1 \qquad (1)$$

where τ is extra stress tensor, p is the pressure, $\boldsymbol{I}$ is the identity tensor, α_i (i = 1, 2), β_i (i = 1, 2, 3) are the material constants and A_k (k = 1, 2, 3) are the first Rivlin-Ericksen tensors [38] which are defined by the following equations:

$$A_1 = (\nabla V) \quad (\nabla V)^T \tag{2}$$

$$A_n = \frac{dA_{n-1}}{dt} + A_{n-1}(\nabla V) + A_{n-1}(\nabla V)^T; \qquad n > 1 \tag{3}$$

The introduction of the appropriate terms into the flow model is considered in section 3. The resulting boundary value problem is found to be well-posed and permits a sound methodology for analysing and appraising non-Newtonian effects on the thermo-fluid polymeric transport phenomena via the deployment of suitable dimensionless parameters.

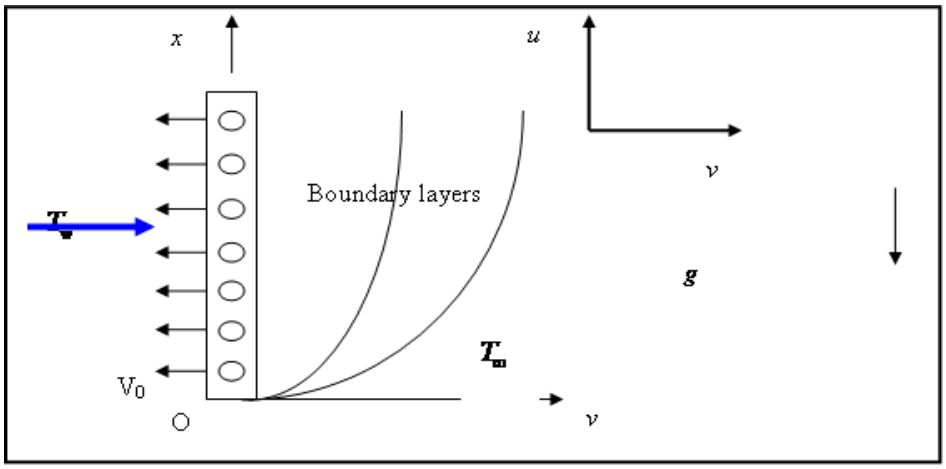

Figure-1: Physical model and coordinate system

3. MATHEMATICAL FLOW MODEL

Steady-state, laminar, double-diffusive, incompressible flow and thermal convection of third grade viscoelastic fluid past a vertical porous plate is considered, as illustrated in **Fig. 1.** The *x* - coordinate is measured from the leading edge of the plate, the *y* - coordinate is measured normal to the plate. The corresponding velocities in *x* and *y* directions are *u* and *v* respectively. The acceleration due to gravity ***g***, acts downwards. We also assume that the Boussinesq approximation holds, i.e., the density variation is experienced solely in the buoyancy term in the momentum equation.

Both plate and the third grade fluid are maintained at the same constant temperature. Instantaneously, it is raised to a temperature $T_w > T_\infty$, the ambient temperature of the fluid which remains unchanged. In line with the approach of Sahoo [9] and Hayat [11-13] and introducing the boundary layer approximations, the equations for *continuity, momentum and energy* can be written as follows:

$$\frac{\partial u}{\partial x} + \frac{\partial v}{\partial y} = 0 \tag{4}$$

$$u\frac{\partial u}{\partial x} + v\frac{\partial u}{\partial y} = \nu\frac{\partial^2 u}{\partial y^2} + \frac{\alpha_1}{\rho}\left[u\frac{\partial^3 u}{\partial x \partial y^2} + v\frac{\partial^3 u}{\partial y^3} + \frac{\partial u}{\partial x}\frac{\partial^2 u}{\partial y^2} + 3\frac{\partial u}{\partial y}\frac{\partial^2 u}{\partial x \partial y}\right] + \frac{2\alpha_2}{\rho}\frac{\partial u}{\partial y}\frac{\partial^2 u}{\partial x \partial y}$$

$$+ \frac{6\beta_3}{\rho}\left(\frac{\partial u}{\partial y}\right)^2\frac{\partial^2 u}{\partial y^2} + g\beta(T - T_\infty) \tag{5}$$

$$u\frac{\partial T}{\partial x} + v\frac{\partial T}{\partial y} = \alpha\frac{\partial^2 T}{\partial y^2} \tag{6}$$

where *u* and *v* are the velocity components in *x* and *y* directions respectively, $\nu = \mu/\rho$ is the kinematic viscosity of the third grade fluid. The *third grade fluid model* introduces a number of *mixed* derivatives into the momentum boundary layer equation (5). The momentum equation therefore attains an order higher than the *classical Navier-Stokes (Newtonian) viscous flow* model. The non-Newtonian effects feature in the shear terms only of eqn. (5) and not the convective (acceleration) terms. The fifth term on the right hand side of eqn. (5) represents the *thermal buoyancy force* and couples the velocity field with the temperature field equation (6).

$$At \quad y = 0, \qquad u = 0, \quad v = -V_w, \quad -k\frac{\partial T}{\partial y} = h_w(T_w - T)$$

$$As \quad y \to \infty, \quad u \to 0, \quad T \to T_\infty \tag{7}$$

Here V_w denotes the uniform transpiration (blowing or suction) velocity at the surface of the plate, T_∞ is the free stream temperature, h_w is the convective heat transfer coefficient, T_w is the convective fluid temperature. The stream function ψ is defined by $u = \frac{\partial \psi}{\partial y}$ and $v = -\frac{\partial \psi}{\partial x}$, and therefore, the continuity equation is automatically satisfied. In order to render the governing equations and the boundary conditions in dimensionless form, the following non-dimensional quantities are introduced.

$$\xi = \frac{V_0 x}{\nu} Gr_x^{-1/4}, \quad \eta = \frac{y}{x} Gr_x^{1/4}, \quad \phi = \frac{16\beta_3 \nu}{\rho x^4} Gr_x^{3/2}, \quad \psi = 4\nu \sqrt[4]{Gr_x} \left(f(\xi,\eta) + \frac{1}{4}\xi \right), \quad \varepsilon_1 = \frac{\alpha_1}{\rho x^2} Gr_x^{1/2}$$
$$\varepsilon_2 = \frac{\alpha_2}{\rho x^2} Gr_x^{1/2}, \quad \Pr = \frac{\nu}{\alpha}, \quad Gr_x = \frac{g\beta_1 (T_w - T_\infty) x^3}{4\nu^2}, \quad \theta(\xi,\eta) = \frac{T - T_\infty}{T_w - T_\infty}, \quad \gamma = \frac{x h_w}{k} Gr_x^{-1/4} \tag{8}$$

All terms are defined in the nomenclature. In view of the transformation defined in eqn. (8), the boundary layer eqns. (5)-(6) are reduced to the following coupled, nonlinear, dimensionless partial differential equations for momentum and energy for the regime:

$$f''' + (3f + \xi) f'' - 2(f')^2 + \varepsilon_1 \left[2f' f''' - (3f + \xi) f^{iv} \right] + (3\varepsilon_1 + 2\varepsilon_2)(f'')^2 - (4\varepsilon_1 + 2\varepsilon_2)\eta f'' f'''$$
$$+6\phi (f'')^2 f''' + \theta = \xi \left[f' \frac{\partial f'}{\partial \xi} - f'' \frac{\partial f}{\partial \xi} - \varepsilon_1 \left(f' \frac{\partial f'''}{\partial \xi} + f''' \frac{\partial f'}{\partial \xi} - f^{iv} \frac{\partial f}{\partial \xi} \right) - (3\varepsilon_1 + 2\varepsilon_2) f'' \frac{\partial f''}{\partial \xi} \right] \tag{9}$$

$$\frac{\theta''}{\Pr} + (3f + \xi)\theta' = \xi \left(f' \frac{\partial \theta}{\partial \xi} - \theta' \frac{\partial f}{\partial \xi} \right) \tag{10}$$

The transformed dimensionless boundary conditions are:

$$\begin{aligned} &At \quad \eta = 0, \qquad f = f_w, \quad f' = 0, \qquad \theta = 1 + \frac{\theta'}{\gamma} \\ &As \quad \eta \to \infty, \quad f' \to 0, \quad \theta \to 0 \end{aligned} \tag{11}$$

Here primes denote the differentiation with respect to η, $\gamma = \frac{x h_w Gr^{-1/4}}{k}$ is the Biot number. The wall thermal boundary condition in (11) corresponds to convective cooling. The skin-friction coefficient (shear stress at the cylinder surface) and Nusselt number (heat transfer rate) can be defined using the transformations described above with the following expressions.

$$Gr^{-3/4} C_f = f''(\xi,0) + \varepsilon_1 \left(5f' f''(\xi,0) - 7ff'''(\xi,0) \right) + 2\phi \left(f''(\xi,0) \right)^3 \tag{12}$$

$$Gr^{-1/4} Nu = -\theta'(\xi,0) \tag{13}$$

The location, $\xi \sim 0$, corresponds to the vicinity of the *lower stagnation point* on the plate.

For this scenario, the model defined by eqns. (9) and (10) contracts to an *ordinary* differential boundary value problem:

$$f''' + 3ff'' - 2(f')^2 + \varepsilon_1 \left[2f' f''' - 3ff^{iv} \right] + (3\varepsilon_1 + 2\varepsilon_2)(f'')^2 - (4\varepsilon_1 + 2\varepsilon_2)\eta f'' f''' + 6\varphi (f'')^2 f''' + \theta = 0 \tag{14}$$

$$\frac{\theta''}{\Pr} + 3f\theta' = 0 \tag{15}$$

The general model is solved using a powerful and unconditionally stable finite difference technique introduced by Keller [33]. The Keller-box method has a second order accuracy with arbitrary spacing and attractive extrapolation features. It converges quickly and is ideal for parabolic problems.

4. COMPUTATIONAL SOLUTION WITH KELLER BOX IMPLICT METHOD

The Keller-Box implicit difference method is implemented to solve the nonlinear boundary value problem defined by eqns. (9)–(10) with boundary conditions (11). This technique, despite recent developments in other numerical methods, remains a powerful and very accurate approach for parabolic boundary layer flows. It is unconditionally stable and achieves exceptional accuracy [33]. Recently this method has been deployed in resolving many challenging, multi-physical fluid dynamics problems. Applications include Casson non-Newtonian fluids [39], oblique micropolar stagnation flows [40], Walter's viscoelastic flows [41], micropolar nanofluids [42], Jeffrey's viscoelastic boundary layers [43], magnetized Williamson fluids [44], nanofluid transport from a sphere [45], Eyring-Powell fluid model [46], Tangent-Hyperbolic fluid model [47] and Maxwell fluids [48]. The Keller-Box discretization is *fully coupled* at each step which reflects the physics of parabolic systems – which are also fully coupled. Discrete calculus associated with the Keller-Box scheme has also been shown to be fundamentally different from all other mimetic (physics capturing) numerical methods, as elaborated in Bég [49]. The Keller Box Scheme comprises four stages.

1) Decomposition of the N^{th} order partial differential equation system to N first order equations.
2) Finite Difference Discretization.
3) Quasilinearization of Non-Linear Keller Algebraic Equations and finally.
4) Block-tridiagonal Elimination solution of the Linearized Keller Algebraic Equations.

5. NUMERICAL RESULTS AND INTERPRETATION

Comprehensive numerical solutions have been obtained and are presented in **Tables 1 - 2** and **Figs.2–10**. The numerical problem comprises two independent variables (ξ,η), two dependent fluid dynamic variables (f,θ) and six rheological and thermo-physical parameters, viz., ϕ, ε_1, ε_2, γ, Pr, ξ. The following default parameter values are deployed: $\phi = 0.1$, $\varepsilon 1 = \varepsilon 2 = 0.3$, $\gamma = 0.2$, $Pr = 0.71$*(low density polymeric solvents)* and $\xi = 1.0$. Furthermore, the influence of stream-wise (transverse) coordinates on flow and temperature characteristics are also investigated.

Table-1: Values of $f''(\xi,0)$ and $-\theta'(\xi,0)$ for different ϕ, ε_1 and ε_2 (Pr = 0.71, γ = 0.2, ξ = 1.0)

ε_1	ε_2	ϕ = 0.0		ϕ = 5.0		ϕ = 10.0		ϕ = 15.0		ϕ = 20.0		ϕ = 30.0	
		C_f	Nu	C_f	Nu	C_f	Nu	C_f	Nu	C_f	Nu	C_f	Nu
0.1	0.3	0.4590	0.5890	0.5497	0.5805	0.5676	0.5761	0.5786	0.5731	0.5866	0.5708	0.5982	0.5674
0.35		0.3523	0.5724	0.4932	0.5699	0.5357	0.5679	0.5563	0.5662	0.5691	0.5648	0.5862	0.5624
0.64		0.2952	0.5620	0.4066	0.5604	0.4698	0.5596	0.5067	0.5588	0.5305	0.5581	0.5593	0.5567
0.87		0.2714	0.5567	0.3498	0.5547	0.4137	0.5543	0.4569	0.5539	0.4876	0.5534	0.5275	0.5526
1.12		0.2574	0.5526	0.3026	0.5498	0.3605	0.5495	0.4042	0.5493	0.4379	0.5491	0.4858	0.5486
1.5		0.2509	0.5485	0.2518	0.5439	0.2980	0.5438	0.3367	0.5437	0.3692	0.5436	0.4203	0.5433
0.3	0	0.3585	0.5743	0.4978	0.5714	0.5612	0.5803	0.5541	0.5672	0.5661	0.5657	0.5821	0.5632
	1	0.3945	0.5760	0.5368	0.5729	0.5724	0.5706	0.5885	0.5685	0.5979	0.5669	0.6108	0.5641
	2	0.4781	0.5784	0.5855	0.5748	0.6180	0.5721	0.6323	0.5697	0.6382	0.5681	0.6468	0.5656
	3	0.5629	0.5797	0.6346	0.5758	0.6662	0.5731	0.6784	0.5711	0.6834	0.5695	0.6881	0.5668
	4	0.6801	0.5811	0.6826	0.5769	0.7079	0.5741	0.7176	0.5718	0.7216	0.5699	0.7252	0.5672
	5	0.7205	0.5826	0.7499	0.5792	0.7772	0.5766	0.7760	0.5742	0.7703	0.5719	0.7635	0.5684

In Table 1, we observe that with increasing ϕ values, skin friction is elevated whereas heat transfer rate (local Nusselt number). Furthermore, an increase in ε_1 reduces skin friction number and heat transfer rate. And an increase in ε_2 is observed to increase both skin friction and heat transfer rate. **Table 2** presents the influence of the *Biot number (*γ) and the Prandtl number (Pr) on skin friction and heat transfer rate along with a variation in the third grade fluid parameter (ϕ). Both Skin friction and heat transfer rate are increased with increasing γ values. Whereas, increasing enhances the skin friction and heat transfer rate. With increasing Pr values (corresponding to denser polymer and solvent suspensions), the skin friction is significantly reduced, whereas heat transfer rate is markedly elevated.

Table-2: Values of $f''(\xi,0)$ and $-\theta'(\xi,0)$ for different γ , Pr and ϕ $\left(\varepsilon_1 = 0.3, \varepsilon_2 = 0.3, \xi = 1.0\right)$

γ	Pr	ϕ = 0.0		ϕ = 5.0		ϕ = 10.0		ϕ = 15.0		ϕ = 20.0		ϕ = 30.0	
		C_f	*Nu*	C_f	*Nu*	C_f	*Nu*	C_f	*Nu*	C_f	*Nu*	C_f	*Nu*
0.3	0.71	0.2677	0.3704	0.3398	0.3695	0.3679	0.3687	0.3826	0.3680	0.3919	0.3674	0.4036	0.3663
0.4		0.3311	0.4972	0.4450	0.4951	0.4791	0.4934	0.4958	0.4920	0.5064	0.4908	0.5202	0.4889
0.5		0.3673	0.5749	0.5076	0.5718	0.5443	0.5695	0.5621	0.5676	0.5736	0.5660	0.5893	0.5634
0.6		0.3908	0.6273	0.5490	0.6235	0.5873	0.6206	0.6058	0.6183	0.6178	0.6164	0.6345	0.6134
1.8		0.4195	0.6934	0.6004	0.6885	0.6404	0.6850	0.6599	0.6822	0.6733	0.6799	0.6912	0.6764
1.0		0.4364	0.7334	0.6311	0.7278	0.6720	0.7238	0.6927	0.7207	0.7060	0.7182	0.7246	0.7143
0.5	0.5	0.4320	0.4468	0.6177	0.4427	0.6565	0.4397	0.6769	0.4374	0.6901	0.4365	0.7082	0.4327
	1	0.3018	0.7516	0.3974	0.7500	0.4317	0.7487	0.4489	0.7475	0.4596	0.7465	0.6806	0.2911
	2	0.1674	1.3952	0.1877	1.3946	0.2050	1.3954	0.2176	1.3960	0.2271	1.3965	0.2404	1.3972
	3	0.0995	2.0874	0.0999	2.0830	0.1051	2.0832	0.1099	2.0836	0.1144	2.0840	0.1221	2.0848
	5	0.0485	3.4967	0.0430	3.4810	0.0434	3.4804	0.0439	3.4805	0.0445	3.4807	0.0458	3.4813
	7	0.0309	4.9049	0.0247	4.8767	0.0245	4.8754	0.0245	4.8756	0.0246	4.8761	0.0248	4.8771

Figures 2(a) – 2(b) depict the velocity $\left(f'\right)$ and temperature $\left(\theta\right)$ distributions with increasing *third grade fluid parameter* (ϕ) through the boundary layer regime. There is a strong elevation (Fig. 2(a)) in linear velocity closer to the plate surface with increase in ϕ. Momentum boundary layer thickness is therefore decreased with greater third order viscoelastic parameter. The mathematical model reduces to the *Newtonian viscous flow model* as $\phi \to 0$, $\varepsilon_1 \to 0$ *and* $\varepsilon_2 \to 0$. In other words, all three viscoelastic material parameters must vanish to retrieve the Newtonian flow case. The momentum boundary layer equation (9) in this case contracts to the familiar equation for *Newtonian mixed convection* from a plate, viz. $f'''+\left(3f+\xi\right)f''-2f'^2+\theta=\xi\left(f'\frac{\partial f'}{\partial \xi}-f''\frac{\partial f}{\partial \xi}\right)$ (16)

The thermal boundary layer equation (10) remains unchanged. Greater third order material effects therefore serve to marginally thicken thermal boundary layers. The third grade material parameter, ϕ is given by $\frac{\beta_3 \nu}{\rho x^4} Gr_x^{3/2}$, where $Gr_x = \frac{g\beta(T_w - T_\infty)x^3}{\nu^2}$ is the local thermal Grashof number. On careful inspection of the parameter, ϕ is directly proportional to the third grade material parameter (β_3) and inversely proportional to the square of kinematic viscosity (ν^2). Therefore, greater ϕ values correspond to stronger third grade material properties (greater elasticity of the liquid) and lower viscosity of the fluid. This will result in an acceleration in the boundary layer flow i.e. grater f' values as observed in fig. 2(a). The parameter ϕ arises actually in a single term in the linear momentum equ. (9), viz $+6\phi(f'')^2 f'''$, and is therefore strongly related to shear rate. As this parameter is increased the fluid requires a lesser shear to flow and stronger elastic effects are present which encourage flow acceleration. The effect is most prominent near the surface of the plate and is in fact reversed further towards the freestream. However, the acceleration effect in the near-wall region is substantially greater than the retardation effect in the edge of the boundary layer i.e. the latter is a weaker phenomenon. Similarly, the temperature field (eqn. 10) is indirectly influenced by the parameter ϕ again owing to coupling with linear momentum eqn. (9) via the thermal buoyancy term (θ). There is a slight increase in temperature magnitudes (Fig. 2(b)) with an increase in ϕ. The thermal boundary layer thickness is therefore enhanced with greater rheological effect. The decrease in viscosity associated with greater ϕ values implies that momentum diffusion rate is lower relative to thermal diffusion rate in the boundary layer. This results in elevated heat diffusion which causes temperatures to increase. In the constitutive eqn. (1), Truesdell and Noll [37] have shown that for proper description of third grade fluids, if all the motions of such liquids are to be compatible with thermodynamics in the sense that these motions meet the Clausius-Duhem inequality and if it is assumed that the specific Helmholtz free energy is a minimum when the fluid is locally at rest, then the following conditions must hold:

$$\mu \geq 0, \alpha_1 \geq 0, \left|\alpha_1 + \alpha_2\right| \leq \sqrt{24\mu\beta_3}, \beta_1 = \beta_2 = 0, \beta_3 \geq 0. \tag{17}$$

The specification of $\varepsilon_1=\varepsilon_2 = 0.3$ as defined in eqn. (8) relates to the prescription of the material moduli values α_1, α_2 in the Reiner-Rivlin third grade viscoelastic model i.e. eqn (17). Evidently also the third grade material parameter (β_3) can have values greater or equal to zero, resulting in ϕ values dependent on the particular selection. Based on consistency with the work of Akyildiz *et al.* [50], Bég *et al*. [51], we study *weakly elastic fluids* as characteristic of solvents and specify $\varepsilon_1=\varepsilon_2 = 0.3$.

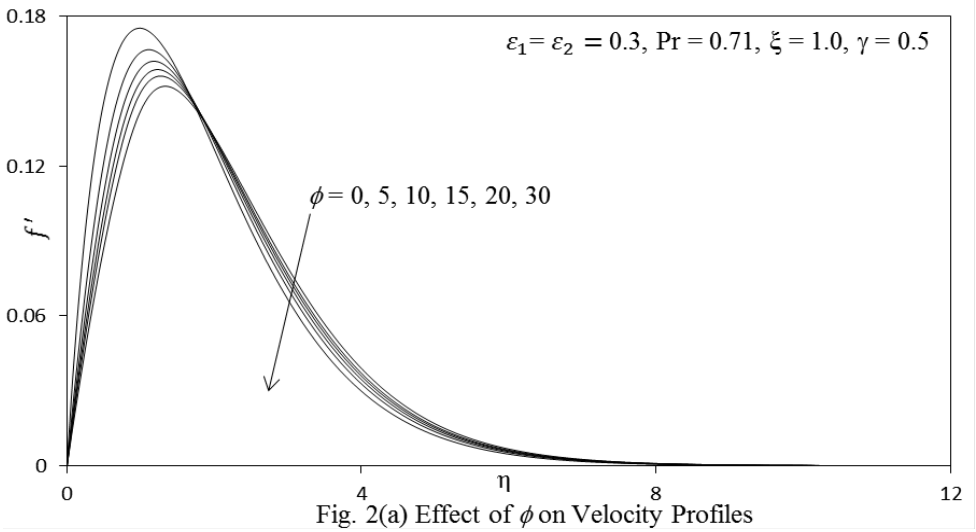

Fig. 2(a) Effect of ϕ on Velocity Profiles

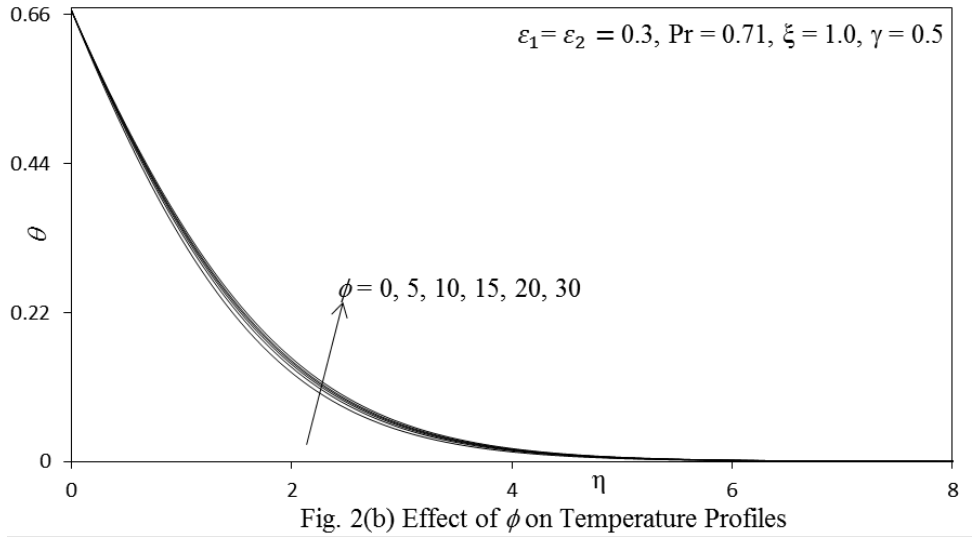

Fig. 2(b) Effect of ϕ on Temperature Profiles

Figures 3(a) - 3(b) illustrates the effect of the *first material fluid parameter*, ε_1, on the velocity $\left(f'\right)$ and temperature $\left(\theta\right)$ distributions through the boundary layer regime. The parameter ε_1, is directly proportional to *first material viscoelastic modulus*, α_1. It appears in numerous terms in the linear momentum eqn. (9). As this parameter increases the relative influence of viscosity also decreases and elasticity in the fluid increases. The reduction in viscosity aids momentum transfer and accelerates the boundary layer flow on the plate surface, resulting in an elevation in linear velocity (fig. 3a). This simultaneously decreases the linear momentum boundary layer thickness. Further, from the wall the opposite behaviour is computed. This is probably due to the relaxation in the rheological fluid with further separation from the plate surface. This results in a shear-thickening in the fluid and higher viscosity which slows the boundary layer flow in this region leading to an in momentum boundary layer thickness. Fig.3b shows that temperatures are consistently enhanced throughout the boundary layer regime with greater ε_1 values. The reduction in liquid viscosity results in energy diffusion rate exceeding the momentum diffusion rate which heats the boundary layer and increases thermal boundary layer thickness.

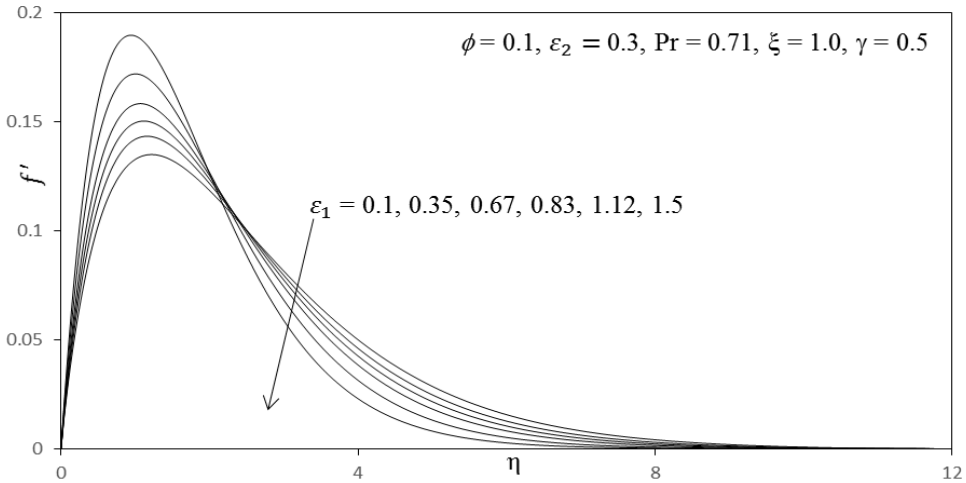

Fig. 3(a) Effect of ε_1 on Velocity Profiles

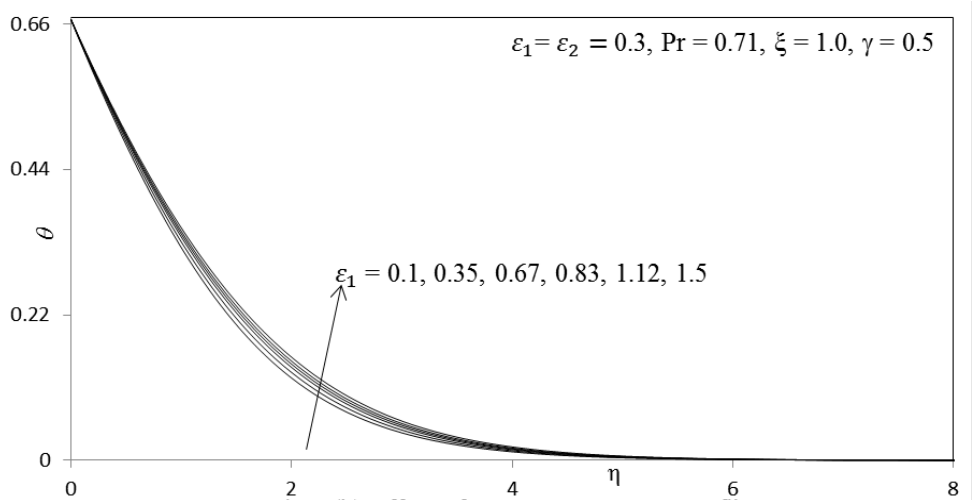

Fig. 3(b) Effect of ε_1 on Temperature Profiles

Figures 4(a) - 4(b) illustrates the effect of the *second material fluid parameter,* ε_2, on the velocity $\left(f'\right)$ and temperature $\left(\theta\right)$ distributions through the boundary layer regime. Dimensionless velocity component is observed to be substantially enhanced with increasing ε_2 values. The definitions of ε_1 and ε_2 only differ in the material modulus (α_1 and α_2) included. However, the influence on thermo-fluid characteristics is very different. Acceleration is consistently achieved with greater ε_2 values, at any location in the boundary layer transverse to the plate surface (fig. 4a), in contrast to increasing ε_1 (fig. 3a) where a different response is induced depending on the location in the boundary layer. Larger ε_2 values correspond therefore to an effective reduction in viscosity of the liquid and greater elasticity. Contrary to fig. 3b, where temperatures are elevated with higher ε_1 values, in fig. 4b we observe that temperatures are reduced with large ε_2 values. Heat diffusion rate is therefore lowered with higher ε_2 values indicating that thermal boundary layer thickness is lowered.

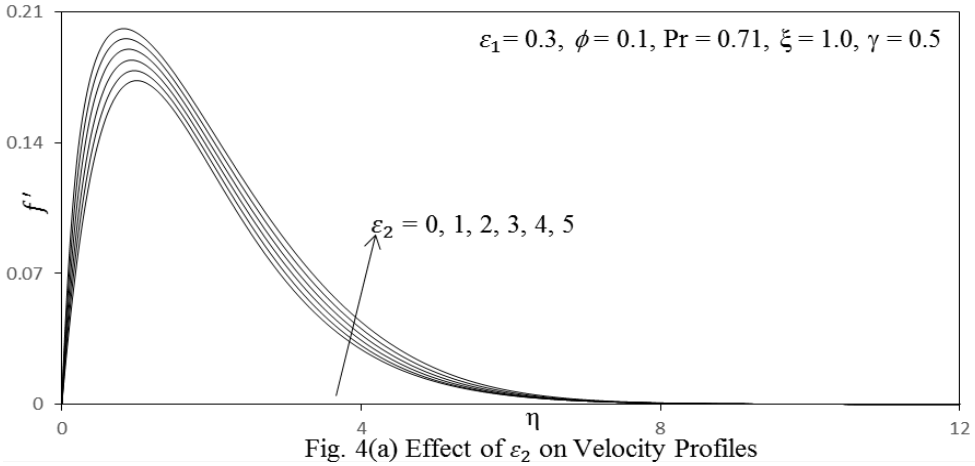

Fig. 4(a) Effect of ε_2 on Velocity Profiles

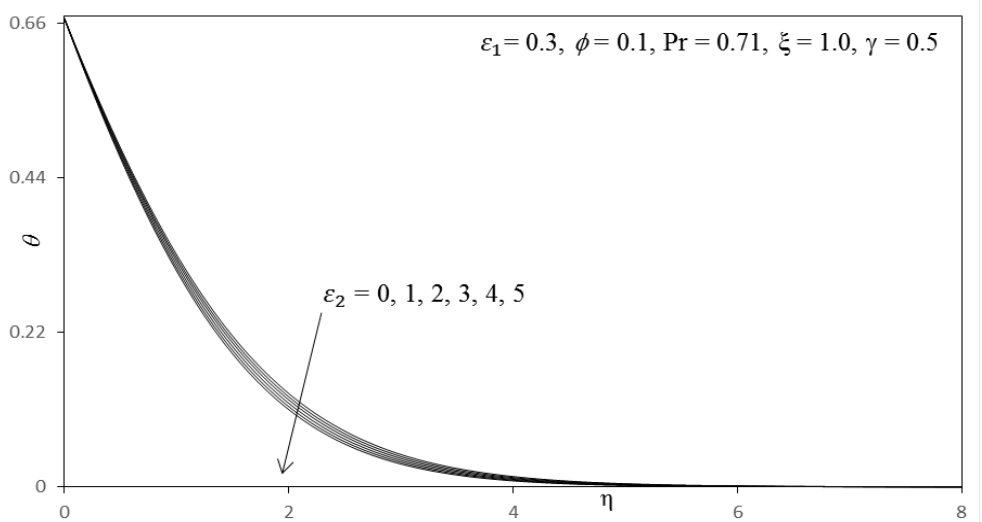

Fig. 4(b) Effect of ε_2 on Temperature Profiles

Figures 5(a) - 5(b) depict the evolution of velocity $\left(f'\right)$ and temperature $\left(\theta\right)$ functions with a variation in Biot number, γ. Dimensionless velocity component (fig. 5a) is considerably enhanced with increasing γ. In fig. 5b, an increase in Biot number is seen to considerably enhance temperatures throughout the boundary layer regime. For $\gamma < 1$ i.e. small Biot numbers, the regime is frequently designated as being "thermally simple" and there is a presence of more uniform temperature fields inside the boundary layer and the cylinder solid surface. For $\gamma > 1$ thermal fields are anticipated to be non-uniform within the solid body. The Biot number effectively furnishes a mechanism for comparing the conduction resistance within a solid body to the convection resistance external to that body (offered by the surrounding fluid) for heat transfer. We also note that a Biot number in excess of 0.1, as studied in figs. 5a, b corresponds to a "thermally thick" substance whereas Biot number less than 0.1 implies a "thermally thin" material. Since γ is inversely proportional to thermal conductivity (k), as γ increases, thermal conductivity will be reduced at the cylinder surface and this will lead to a decrease in the rate of heat transfer from the boundary layer to within the cylinder, manifesting in a rise in temperature at the cylinder surface and in the body of the fluid- the maximum effect will be sustained at the surface, as witnessed in fig. 5b. However for a fixed wall convection coefficient and thermal conductivity, Biot number as defined in $\gamma = \frac{xh_w}{k} Gr^{-1/4}$ is also directly inversely proportional to the local Grashof (free convection) number. As local Grashof number increases generally the enhancement in buoyancy causes a deceleration in boundary layer flows [52, 53]; however as Biot number increases, the local Grashof number must decreases and this will induce the opposite effect i.e. accelerate the boundary layer flow, as shown in fig. 5a.

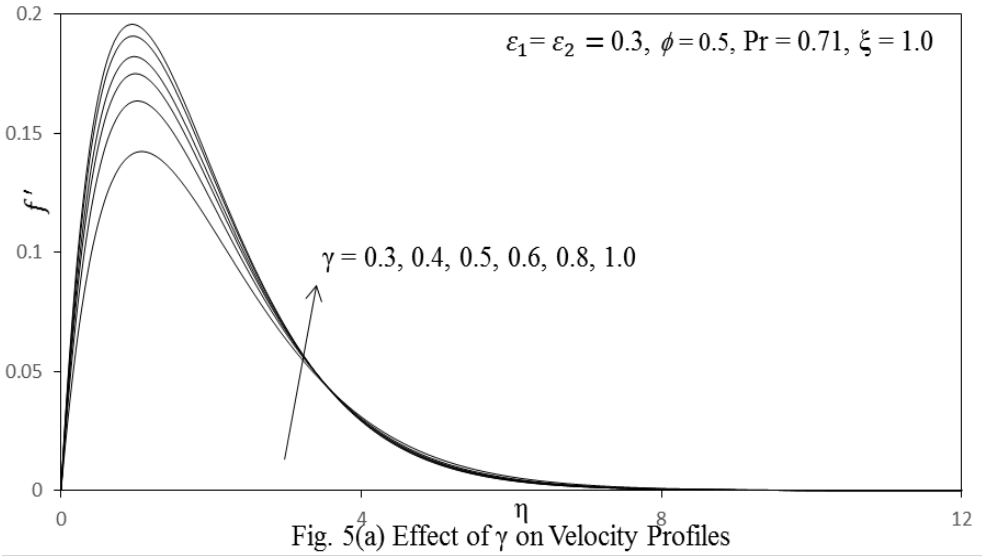

Fig. 5(a) Effect of γ on Velocity Profiles

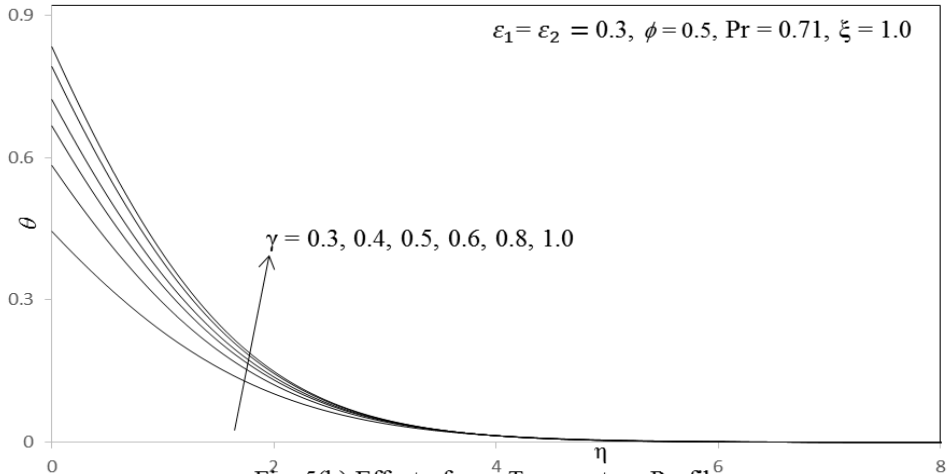

Fig. 5(b) Effect of γ on Temperature Profiles

Figures 6(a) – 6(b) depicts the velocity (f') and temperature (θ) distributions with radial coordinate, for various transverse (stream wise) coordinate values, ξ along with the variation in the third grade fluid parameter (ϕ). This parameter also embodies the local Grashof number and can be viewed as a free convection parameter as elaborated by Gorla *et al*. [54]. Clearly, from fig. 6(a) it can be seen that as suction parameter ξ increases, the maximum fluid velocity decreases. This is due to the fact that with greater suction values, the flow location moves further along the plate surface from the apex towards the broad periphery of the plate. Buoyancy forces increase as this occurs and this suppress momentum diffusion, leading to deceleration in the flow and a thicker boundary layer structure. Fig. 6(b) shows the effect of the increasing ξ values on the temperature profiles. All the temperature profiles decay smoothly from the maximum at the plate surface to the minimum in the free stream. With progressive distance from the leading edge, the fluid is therefore cooled and thermal boundary layer thickness decreases. It is also seen that an increase in ϕ, the impedance offered by the fibers of the will increase and this will effectively decelerate the flow in the regime, as testified to by the evident decrease in velocities shown in fig. 6(a).

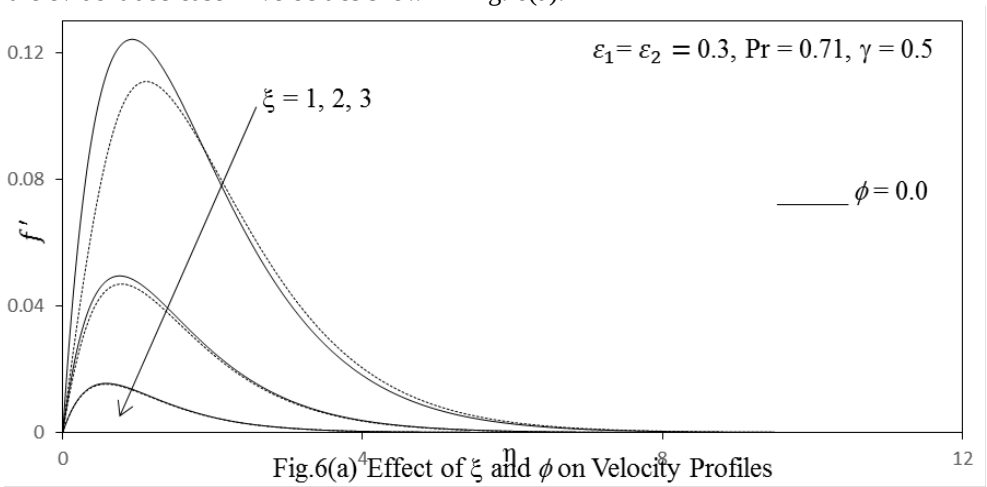

Fig.6(a) Effect of ξ and ϕ on Velocity Profiles

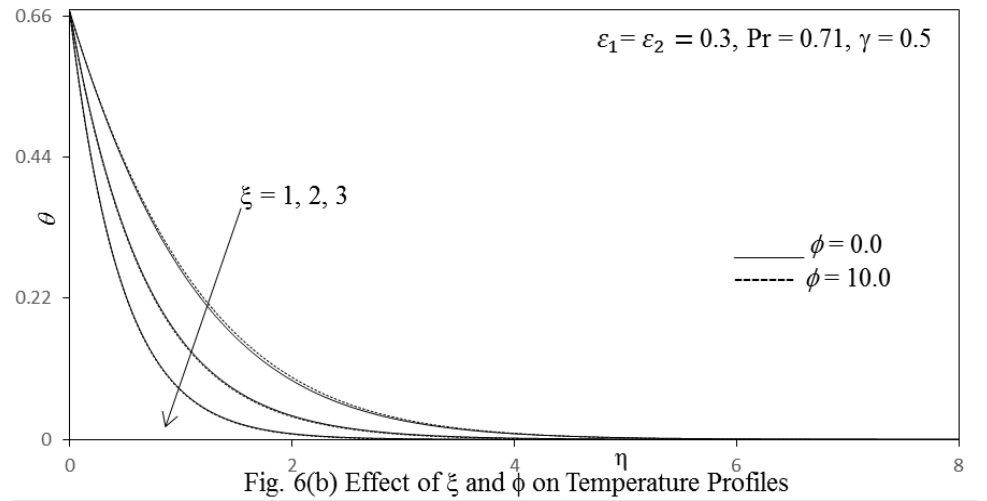

Fig. 6(b) Effect of ξ and ϕ on Temperature Profiles

Figures 7(a) – 7(b) depict the velocity (f') and temperature (θ) distributions with radial coordinate, for various transverse (stream wise) coordinate values, ξ along with the variation in the material parameter (ε_1). Clearly, from these figures it can be seen that as suction parameter ξ increases, the maximum fluid velocity decreases. This is due to the fact that the effect of the suction is to take away the warm fluid on the vertical plate and thereby decrease the maximum velocity with a decrease in the intensity of the natural convection rate. Fig. 7(b) shows the effect of the local suction parameter on the temperature profiles. It is noticed that the temperature profiles decrease with an increase in the suction parameter and as the suction is increased, more warm fluid is taken away and this the thermal boundary layer thickness decreases. It is also seen that an increase in ε_1, the impedance offered by the fibres of the porous medium will increase and this will effectively decelerate the flow in the regime, as testified to by the evident decrease in velocities shown in fig. 7(a).

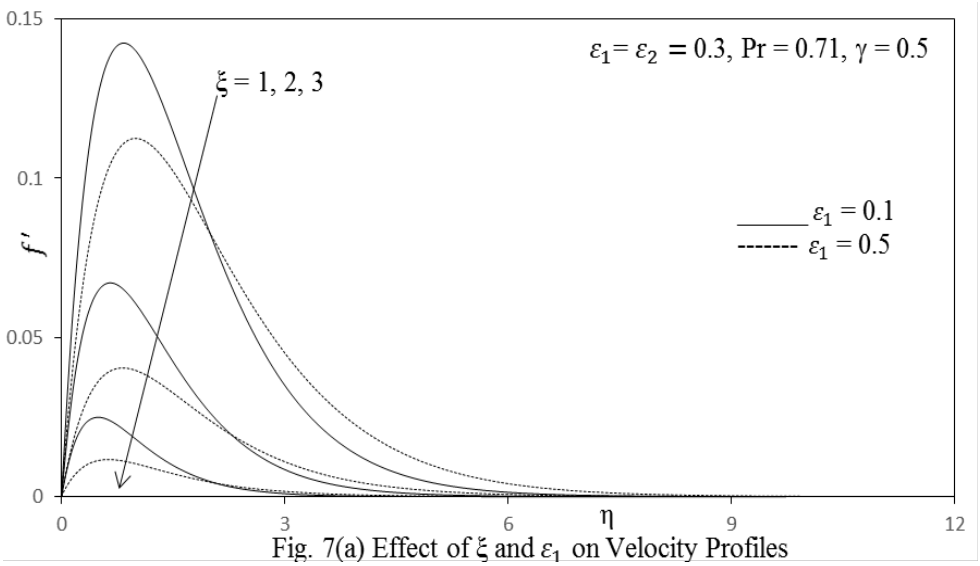

Fig. 7(a) Effect of ξ and ε_1 on Velocity Profiles

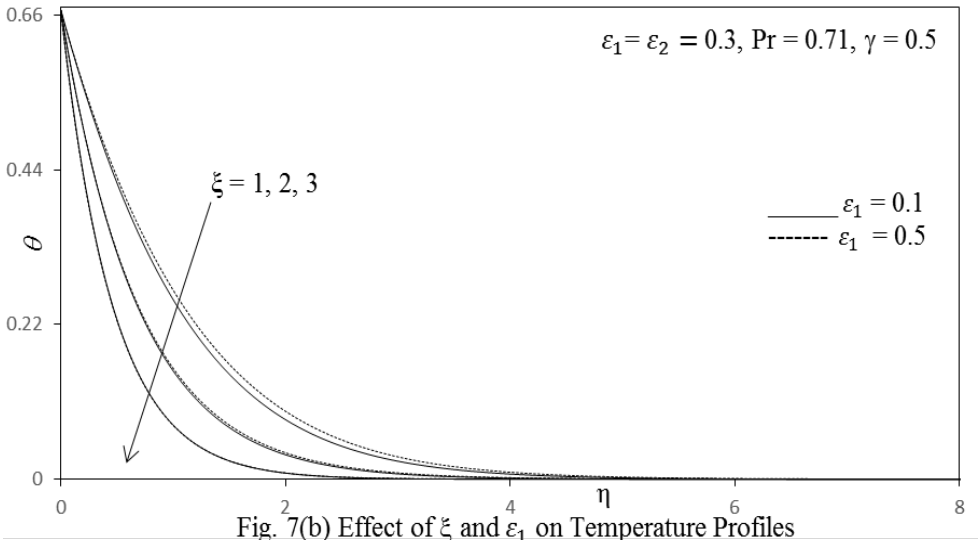

Fig. 7(b) Effect of ξ and ε_1 on Temperature Profiles

Figures 8(a) – 8(b) depict the influence of the third grade dimensionless material parameter, ϕ, on the dimensionless skin friction (C_f) and the heat transfer rate i.e. Nusselt number (Nu) at the plate surface. It is observed in fig. 8(a) that the C_f is elevated with an increase in ϕ. This concurs with earlier graphs described previously, since higher skin friction corresponds to greater acceleration and larger vales of third grade material parameter are known to reduce viscosity effects and enhance momentum diffusion. Conversely, the surface heat transfer rate (fig. 8(b)) is reduced substantially with increasing ϕ which again correlates will temperature computations discussed previously. Since temperatures decrease with greater third grade material viscoelastic effect, heat transfer to the wall must also fall (heat transfer is enhanced to the body of fluid) and this explains why Nusselt number magnitudes are reduced.

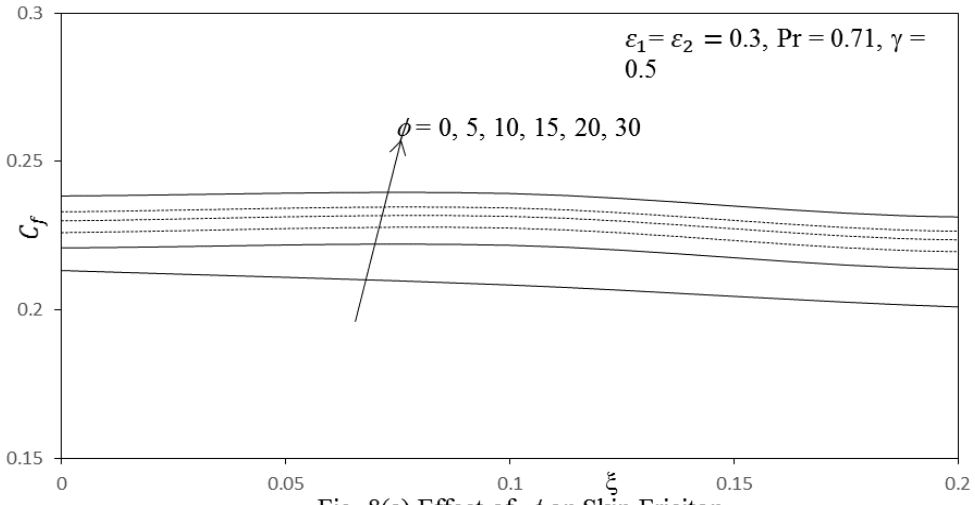

Fig. 8(a) Effect of ϕ on Skin Friciton

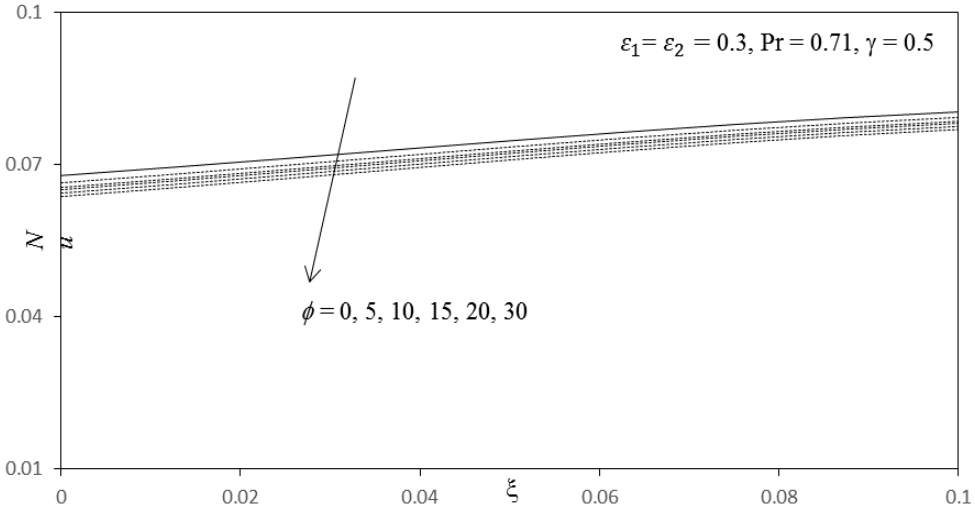

Fig. 8(b) Effect of ϕ on Nusselt number

Figures 9(a) – 9(b) illustrate the effect of the material fluid parameter ε_1 on the dimensionless skin friction (C_f) and heat transfer rate (N_u) at the plate surface. It is observed that the C_f and N_u are depressed strongly along the entire plate surface i.e. for all values of ξ, with an increase in ε_1. The first viscoelastic material modulus parameter, as studied earlier, decelerates the linear flow whereas it raises temperatures. This is entirely consistent with the solutions fives in figs. 9(a) – (b) wherein skin friction and wall heat transfer rate are depressed. Linear acceleration corresponds to lower shear stresses. Increasing temperatures imply that heat transfer rate to the wall must be decreased.

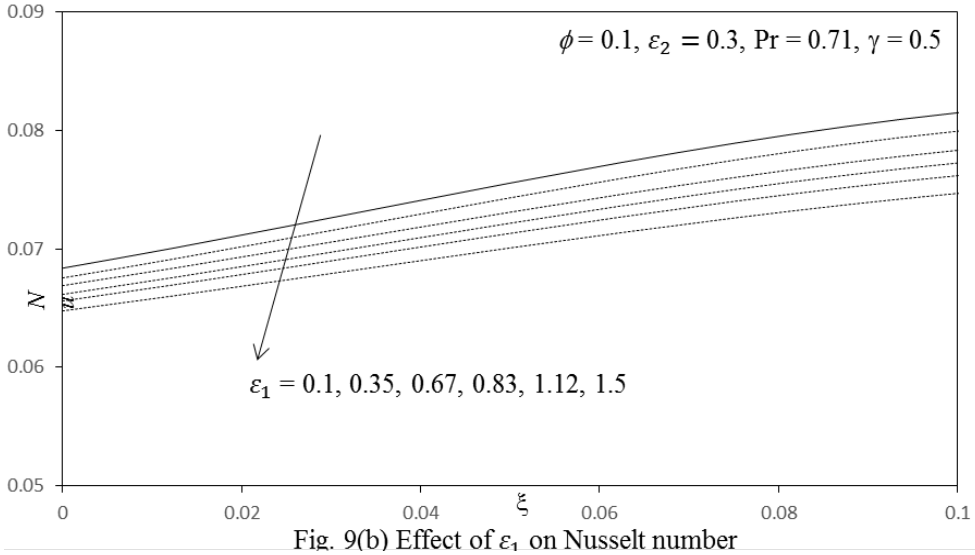

Fig. 9(b) Effect of ε_1 on Nusselt number

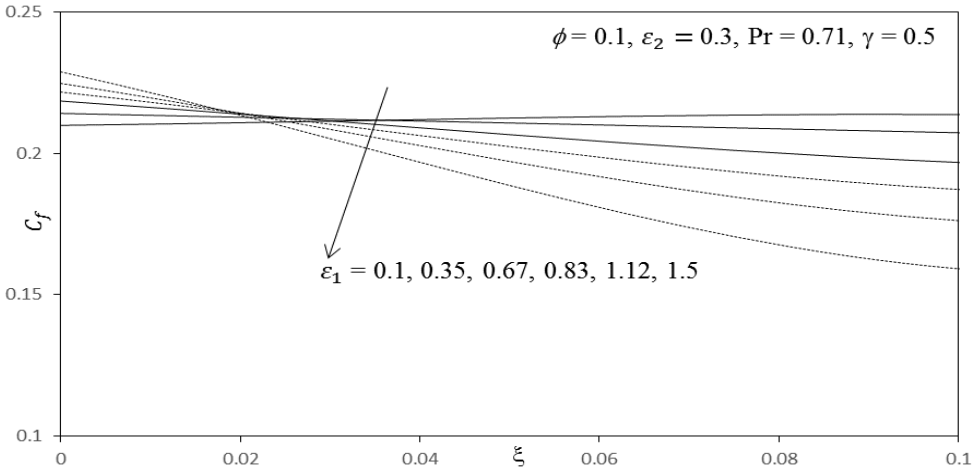

Fig. 9(a) Effect of ε_1 on Skin Friction

Figures 10(a) - 10(b) presents the influence of the Biot number, γ, on the dimensionless skin friction (C_f) and heat transfer rate (N_u) at the plate surface. The skin friction at the plate surface is found to be greatly enhanced with rising γ. This is principally attributable to the decrease in Grashof (free convection) number which results in an acceleration in the boundary layer flow. Heat transfer rate (local Nusselt number) is also enhanced with increasing γ, at large values of ξ, as computed in fig.10(b).

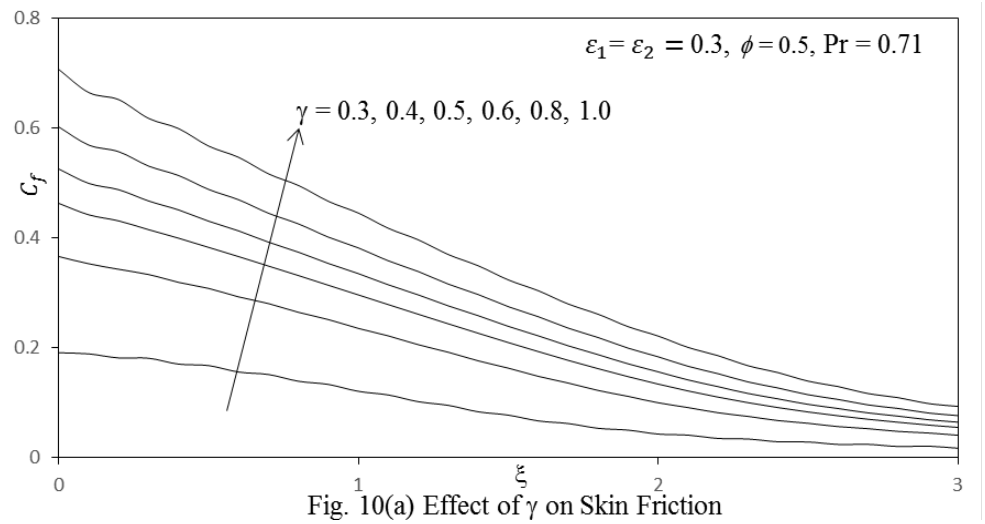

Fig. 10(a) Effect of γ on Skin Friction

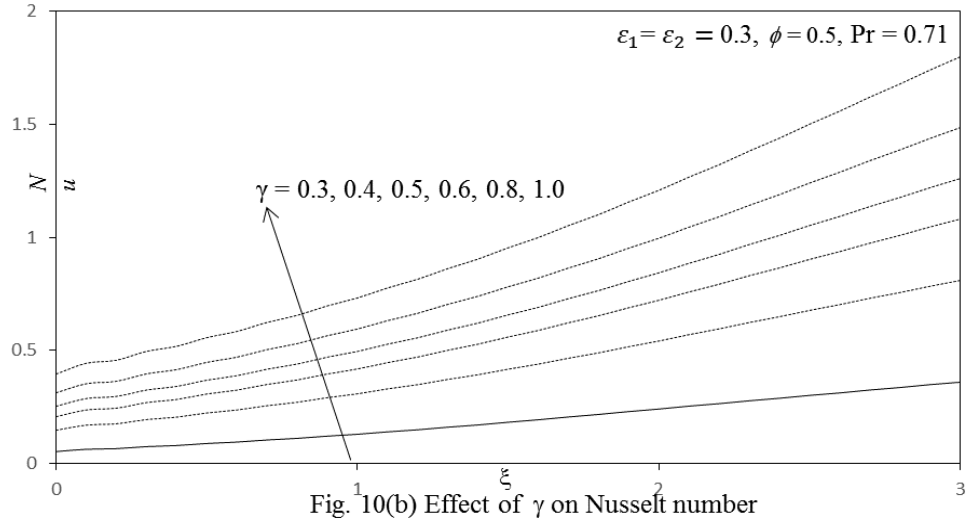

Fig. 10(b) Effect of γ on Nusselt number

6. CONCLUSIONS

Numerical solutions have been presented for the buoyancy-driven, non-similar convective boundary layer flows of third grade viscoelastic non-Newtonian fluid external to a vertical plate. The Keller-box implicit second order accurate finite difference numerical scheme has been utilized to efficiently solve the transformed, dimensionless velocity and thermal boundary layer equations, with prescribed boundary conditions. A comprehensive assessment of the effects of the third grade parameter (ϕ), first and second viscoelastic material fluid parameters (ε_1, ε_2), Prandtl number (Pr) and also the streamwise coordinate (ξ) on thermo-fluid characteristics has been conducted. Very stable and accurate solutions are obtained with the present finite differences code. The computations have shown that the different third grade rheological parameters exert a varied influence on velocity and temperature and also on the gradients of these functions (i.e. skin friction and Nusselt number). skin friction and Nusselt number are markedly reduced along the entire cone surface i.e. for all values of ξ, with greater values of first viscoelastic material parameter (ε_1) whereas increasing second viscoelastic material parameter (ε_2) boosts the skin friction and weakly increases Nusselt number. Increasing third grade material parameter (ϕ) is found to increase linear velocity (and skin friction) and weakly increase temperatures. Increasing stream-wise coordinate (ξ) decelerates the boundary layer flow and cools the boundary layer. Increasing Biot number (γ) enhances linear velocity, temperature, skin friction and heat transfer rate. The numerical Keller box code is able to solve nonlinear rheological boundary layer flow problems very efficiently and therefore shows excellent promise in simulating transport phenomena in other non-Newtonian fluids. In this regard it is being explored with other non-Newtonian formulations and the results of these studies will be communicated imminently.

7. REFERENCES

[1] Fetecau, C., Mahmood, A., and Jamil, M. Exact solutions for the flow of a viscoelastic fluid induced by a circular cylinder subject to a time dependent shear stress, *Comm. Nonlinear Science and Numerical Simulation*, 15(12), 3931–3938 (2010).

[2] Jamil, M., Fetecau, C., and Imran, M. Unsteady helical flows of Oldroyd-B fluids, *Comm. Nonlinear Science and Numerical Simulation*, 16(3), 1378–1386 (2011).

[3] Tan, W. C. and Masuoka, T. Stability analysis of a Maxwell fluid in a porous medium heated from below. *Physics Letters A*, 360(3), 454–460 (2007).

[4] Tan, W. C. and Masuoka, T. Stokes first problem for an Oldroyd-B fluid in a porous half space. *Physics of Fluids*, 17(2), 023101–023107 (2005).

[5] V. R. Prasad, A Subba Rao, N Bhaskar Reddy, B Vasu and O Anwar Bég, Modelling laminar transport phenomena in a Casson rheological fluid from a horizontal circular cylinder with partial slip, *Proc IMechE Part E: J Process Mechanical Engineering*, 227, 309-326 (2013).

[6] M. K. Chaube, D. Tripathi, O. Anwar Bég, S. Sharma and V.S. Pandey, Peristaltic creeping flow of power-law physiological fluids through a non-uniform channel with slip effect, *Applied Bionics and Biomechanics*, Vol. 2015, Article ID 152802, 10 pages. http://dx.doi.org/ 10.1155/ 2015/152802.

[7] P.V. Satya Narayana, D, Harish Babu, Numerical study of MHD heat and mass transfer of a Jeffrey fluid over a stretching sheet with chemical reaction and thermal radiation, *Journal of the Taiwan Institute of Chemical Engineers*, Vol. 59, pp.18-25, 2016.

[8] S. Hina, MHD peristaltic transport of Eyring-Powell fluid with heat/mass transfer, wall properties and slip conditions, *Journal of Magnetism and Magnetic Materials*, Vol. 404, pp.148-158, 2016.

[9] B. Sahoo, S. Poncet, Flow and heat transfer of third grade fluid past an exponentially stretching sheet with partial slip boundary conditions, *Int. J. Heat and Mass Transfer*, 54, 23-24, 5010-5019 (2011).

[10] A. Aziz and T. Aziz, MHD flow of a third grade fluid in porous half space with plate suction or injection: An analytical approach, *Applied Mathematics and Computation*, 218, 21, 10443-1045 (2012).

[11] T. Hayat, A. Shafiq, A. Alsaedi, M. Awais, MHD axisymmetric flow of third grade fluid between stretching sheets with heat transfer, *Computers & Fluids*, 86, 103-108 (2013).

[12] Hayat T., Zahid Iqbal, Meraj Mustafa and Awatif A. Hendi, Melting heat transfer in the stagnation-point flow of third grade fluid past a stretching sheet with viscous dissipation, *Thermal Science*, 17, 865-875 (2013).

[13] Hayat T., Anum Shafiq, A. Alsaedi, MHD axisymmetric flow of third grade fluid by a stretching cylinder, *Alexandria Engineering J.*, 54, 205-212 (2015).

[14] Samuel O. Adesanya, J.A. Falade, Thermodynamic analysis of hydromagnetic third grade fluid flow through a channel filled with porous medium, *Alexandria Engineering J.*, 54, pp.615-622, 2015.

[15] Abdul hameed M., W.Varnhorn, I. Hasim, R. Roslan, The unsteady flow of a third grade fluid caused by the periodic motion of an infinite wall with transpiration, *Alexandria Engineering J.* (2015). http://dx.doi.org/10.1016/j.aej.2015.06.002.

[16] Rashidi M.M., S. Bagheri, E. Momoniat, N. Freidoonimehr, Entropy analysis of convective MDH flow of third grade non-Newtonian fluid over a stretching sheet, *Ain Shams Engineering J.* (2015). http://dx.doi.org/10.1016/j.asej.2015.08.012.

[17] A. Ishak, Similarity solutions for flow and heat transfer over a permeable surface with convective boundary condition, *Appl. Math. Comput*. 217 (2010) 837–842.

[18] A. Aziz, A similarity solution for laminar thermal boundary layer over a flat plate with a convective surface boundary condition, *Comm.Non. Sci. Num. Sim*. 14 (2009) 064–1068.

[19] A. Aziz, Hydrodynamic and thermal slip flow boundary layers over a flat plate with constant heat flux boundary condition, *Comm. Non. Sci. Num. Sim*. 15 (2010) 573–580.

[20] O.D. Makinde, P.O. Olanrewaju, Buoyancy effects on thermal boundary layer over a vertical plate with a convective surface boundary condition, *Trans. ASME J. Fluids Eng*. 132 (2010) 044502-2.

[21] O.D. Makinde, A. Aziz, MHD mixed convection from a vertical plate embedded in a porous medium with a convective boundary condition, *Int. J. Therm. Sci*. 49 (2010) 1813–1820.

[22] D. Gupta, L. Kumar, O Anwar Bég and B. Singh, Finite element simulation of mixed convection flow of micropolar fluid over a shrinking sheet with thermal radiation, *Proc. IMechE. Part E: J Process Mechanical Engineering*, Vol. 228, no. 1, pp.61-72, 2014.

[23] O. D. Makinde, K. Zimba, O. Anwar Bég, Numerical study of chemically-reacting hydromagnetic boundary layer flow with Soret/Dufour effects and a convective surface boundary condition, *Int. J. Thermal and Environmental Engineering*, 4, 89-98 (2012).

[24] O. Anwar Bég, M.J. Uddin, M.M. Rashidi and N. Kavyani, Double-diffusive radiative magnetic mixed convective slip flow with Biot number and Richardson number effects, *J. Engineering Thermophysics* (2013).

[25] S.V.Subhashini, N.Samuel and I. Pop, Double-diffusive convection from a permeable vertical surface under convective boundary condition, *Int. Commun. Heat Mass Transfer*, 38 (2011) 1183-1188.

[26] Sohail Nadeem, Rizwan Ul Haq and Noreen Sher Akbar, MDH three-dimensional boundary layer flow of Casson nanofluid past a linearly stretching sheet with convective boundary condition, *IEEE Transactions on Nanotechnology*, Vol. 13, No. 1, pp. 109-105, 2014.

[27] Ammarah Raees, Hang Xu and Muhammead Raess-ul-Haq, Explicit solutions of wall jet flow subject to a convective boundary condition, *Boundary Value Problems*, 2014, 2014:163. doi:10.1186/1687-2770-2014-163.

[28] Prabhugouda Mallangaouda Patil and E. Momoniat, Influence of convective boundary condition on double diffusive mixed convection from a permeable vertical surface, *Int. J. of Heat and Mass Transfer*, 71 (2014) 313-321.

[29] Fazlina Aman and Anuar Ishak, Mixed convection boundary layer flow towards a vertical plate with convective surface boundary condition, *Mathematical Problems in Engineering*, Article ID 453457, Vol. 2012, 11pages, 2012. DOI:10.1155/2012/453457.

[30] Mohammad M. Rashidi, Mohammad Ferdows, Amir Basiri Parsa and Sjirley Abelman, MHD natural convection with convective surface boundary condition over a flat plate, *Abstract and Applied Analysis*, Vol. 2014, Article ID 923487, 10 pages, 2014. http://dx.doi.org/10.1155/2014/923487.

[31] Rabia Malik, Masood Khan, Asif Munir, Waqar Azeem Khan, Flow and Heat Transfer in Sisko fluid with convective boundary condition, *PLOS ONE*, 9(10): e107989, 2014. Doi:10.1371/journal.pone.0107989.

[32] Makinde O. D., A, Aziz, Boundary layer flow of a nonfluid past a stretching sheet with a convective boundary condition, *Int. J. of Thermal Sciences*, 20 (2011) 1326-1332. doi:10.1016/j.ijthermalsci.2011.02.019.

[33] H.B. Keller, *Numerical Solution of Two-Point Boundary Value Problems*, SIAM Press, Philadelphia, USA (1976).

[34] V. R. Prasad, B. Vasu, O. Anwar Bég and D. R. Parshad, Thermal radiation effects on magnetohydrodynamic free convection heat and mass transfer from a sphere in a variable porosity regime, *Comm. Nonlinear Science Numerical Simulation*, 17, 654–671 (2012).

[35] Bird, R.B., Armstrong, R.C. and Hassager, O., *Dynamics of Polymeric Liquids. Volume 1: Fluid Mechanics*, Vol. 1, 2nd Edition, Wiley Interscience, New York, USA (1987).

[36] Larson, R.G., *Constitutive Equations for Polymer Melts and Solutions, Series in Chemical Engineering*, Butterworths, Boston (1988).

[37] Truesdell C. and Noll W., The non-linear field theories of mechanics, *Handbuch der Physik*, Band III/3, pp. 1–602, Springer, Berlin, Germany (1965).

[38] R. S. Rivlin and J. L. Ericksen, Stress-deformation relations for isotropic materials, *Journal of Rational Mechanics and Analysis*, vol. 4, pp. 323–425, 1955.

[39] V.R. Prasad, A. SubbaRao, N. Bhaskar Reddy, B. Vasu, O. Anwar Bég, Modelling laminar transport phenomena in a Casson rheological fluid from a horizontal circular cylinder with partial slip, *Proc IMechE-Part E: J. Process Mechanical Engineering*, 227 (4) **309-326** (2013).

[40] Y. Y. Lok, I. Pop, D. B. Ingham, Oblique stagnation slip flow of a micropolar fluid, *Meccanica*, 45, 187-198 (2010).

[41] T-B. Chang, A. Mehmood, O. Anwar Bég, M. Narahari, M.N. Islam and F. Ameen, Numerical study of transient free convective mass transfer in a Walters-B viscoelastic flow with wall suction, *Comm. Nonlinear Science and Numerical Simulation*, 16, 216-225 (2011).

[42] V. R. Prasad, S. A. Gaffar and O. Anwar Bég, Heat and mass transfer of a nanofluid from a horizontal cylinder to a micropolar fluid, *AIAA J. Thermophysics Heat Transfer*, 29, 127-139 (2015).

[43] V.R. Prasad, S. Abdul Gaffar, E. Keshava Reddy and O. Anwar Bég, Numerical study of non-Newtonian boundary layer flow of Jeffreys fluid past a vertical porous plate in a Non-Darcy porous medium, *Int. J. Comp. Meth. Engineering Science & Mechanics*, 15 (4) 372-389 **(2014).**

[44] R. M. Darji and M. G. Timol, On invariance analysis of MHD boundary layer equations for non-Newtonian Williamson fluids, *Int. J. Adv. Appl. Math. And Mech*. 1, 10 – 19 (2014).

[45] Ramachandra Prasad V., S. Abdul gaffar and O. Anwar Bég, Non-Similar computational solutions for free convection boundary layer flow of a nanofluid from an isothermal sphere in a Non-Darcy porous medium, *J. Nanofluids*, 4, 1-11 (2015).

[46] S. Abdul Gaffar, V. Ramachandra Prasad, Bhuvana Vijaya, O. Anwar Beg, Mixed convection flow of magnetic viscoelastic polymer from a non-isothermal wedge with Biot number effects, *Int. J of Eng. Maths*, Volume 2015, Article ID 287623, 15 pages, 2015.

[47] S. Abdul Gaffar, V. Ramachandra Prasad, E. Keshava Reddy, Magnetohydrodynamic free Convection flow and heat transfer of non-Newtonian Tangent Hyperbolic fluid from horizontal circular cylinder with Biot number effects, *International Journal of Applied and Computational Mathematics*, 2016, pp.1-23 DOI 10.1007/s40819-015-0130-y

[48] V. Singh, S. Agarwal, Flow and heat transfer of Maxwell fluid with variable viscosity and thermal conductivity over an exponentially stretching sheet, *Amer. J. Fluid Dynamics*, 3, 87-95 (2013).

[49] O. Anwar Bég, Numerical methods for multi-physical magnetohydrodynamics, Chapter 1, pp. 1-112, *New Developments in Hydrodynamics Research*, *Nova Science*, *New York*, *September* (2012).

[50] T. Akyildiz, F., Bellout, H. and Vajravelu, K.: Exact solutions of nonlinear differential equations arising in third grade fluid flows, *Int. J. Non-Linear Mech.*, 39, 1571–1578 (2004).

[51] O. Anwar Bég, H. S. Takhar, R. Bharagava, Rawat, S. and Prasad, V.R., Numerical study of heat transfer of a third grade viscoelastic fluid in non-Darcian porous media with thermophysical effects, *Physica Scripta*, 77, 1-11 (2008).

[52] J.N. Potter and N Riley, Free convection from a heated sphere at large Grashof number, *J. Fluid Mechanics*, 100, 769-783 (1980).

[53] A. Prhashanna, R.P. Chhabra, Free convection in power-law fluids from a heated sphere, *Chem. Eng. Sci*., 65, 6190-6205 (2010).

[54] R. S. R. Gorla, A. Slaouti, H.S. Takhar, Free convection in micropolar fluids over a uniformly heated vertical plate, *Int. J. Numerical Methods for Heat & Fluid Flow*, 8, 504 – 518 (1988).

Source of support: Nil, Conflict of interest: None Declared.